Eur. Phys. J. Special Topics **208**, 133–139 (2012)

DOI: 10.1140/epjst/e2012-01614-y

THE EUROPEAN PHYSICAL JOURNAL SPECIAL TOPICS

Regular Article

Resonant soft X-ray scattering studies of multiferroic YMn_2O_5

S. Partzsch[1,2,a], S.B. Wilkins[2], E. Schierle[3], J.E. Hamann-Borrero[1], H. Wadati[4], V. Soltwisch[3], J.P. Hill[2], E. Weschke[3], D. Souptel[1], B. Büchner[1], and J. Geck[1]

[1] Leibniz Institute for Solid State and Materials Research IFW Dresden, Helmholtzstrasse 20, 01069 Dresden, Germany
[2] Condensed Matter Physics and Material Science Department, Brookhaven National Laboratory, Upton, New York 11973, USA
[3] Helmholtz-Zentrum Berlin für Materialien und Energie, Albert-Einstein-Str. 15, 12489 Berlin, Germany
[4] Department of Applied Physics and Quantum-Phase Electronics Center (QPEC), University of Tokyo, Takeda Frontier Science Hall 202, 2-11-16 Yayoi, Bunkyo-ku, Tokyo 113-0032, Japan

Received 16 December 2011 / Received in final form 23 March 2012
Published online 15 June 2012

Abstract. We performed soft X-ray resonant scattering at the Mn $L_{2,3}$- and OK edges of YMn_2O_5. While the resonant intensity at the Mn $L_{2,3}$ edges reflects the magnetic order parameter, the resonant scattering at the O K edge is found to be directly related to the macroscopic ferroelectric polarization. The latter observation reveals the important role of the spin-dependent Mn-O hybridization for the multiferroicity of YMn_2O_5. We present details about how to obtain correct energy dependent lineshapes and discuss the origin of the resonant intensity at the O K edge.

1 Introduction

Multiferroics are a wide class of materials displaying various interesting properties. For example, large magneto-electric (ME) couplings have gained a lot of attention for possible applications such as a magnetic computer memory that can be switched with an electrical field (see, e.g., [1,2]). However, strong ME coupling is very rare in nature [1,2]. It was therefore greeted with a lot of excitement, when a number of frustrated magnetic transition metal oxide (TMO) compounds were discovered [3,4], where in fact the ferroelectric (FE) polarization, $\mathcal{P}$, is strongly coupled to the magnetic ordering.

The compounds RMn_2O_5 (R = rare earth, Y, Bi) belong to this class of novel multiferroic materials. Here the strong ME coupling is commonly explained by distortions of the ionic lattice, which optimize the energy of the magnetic system by modulations of the ionic positions of Mn and/or O ($\mathcal{P}_{\rm ion}$) [1,2,4]. Recently, however, doubts have been cast that this mechanism alone can fully account for the multiferroic behavior of

[a] e-mail: s.partzsch@ifw-dresden.de

these compounds and another contribution to the ferroelectric polarization, i.e., one due to the valence electrons ($\mathcal{P}_{\rm el}$) of Mn and O, has been discussed [5–9]. Calculations even suggested that in the special case of RMn_2O_5 $\mathcal{P}_{\rm el}$ partially cancels $\mathcal{P}_{\rm ion}$, thus causing a reduction of the macroscopic $\mathcal{P}$ [7].

For YMn_2O_5 we have found that the spin-dependent Mn-O hybridization is a fundamental ingredient for the magnetically driven ferroelectricity [10]. We reached this conclusion by tracking the diffraction peaks by resonant soft X-ray scattering (RSXS) at the Mn $L_{2,3}$- and O K edges. In this article we present additional details of our RSXS studies [10] and elaborate on the origin of the magnetic scattering process at the O K edge.

YMn_2O_5 crystallizes in the space group $Pbam$ with $a = 7.26$ Å, $b = 8.46$ Å, and $c = 5.66$ Å at room temperature [11]. In this structure manganese occupies two different crystallographic sites; the first coordinated by an oxygen octahedron (Mn1) and the second by an oxygen square-based pyramid (Mn2) [11,12]. The Mn1-octahedra form edge-sharing chains along the c-direction that are linked within the ab-plane by Mn2-pyramid dimers. Within an ionic description, the very different local coordination of Mn1 and Mn2 results in different crystal field splittings and, hence, different formal valencies of these two sites, namely $4 + (3d^3)$ for Mn1 and $3 + (3d^4)$ for Mn2 [13].

As a function of temperature, YMn_2O_5 undergoes a sequence of phase transitions, which demonstrate the strong coupling between the magnetic and the FE order: Upon cooling, a transition from paramagnetic to high-temperature incommensurate (HTIC) antiferromagnetic (AFM) occurs at $T_1 = 45$ K [14]. At $T_2 = 39$ K the AFM order becomes commensurate (C) with $\mathbf{q}_{\rm C} = (1/2, 0, 1/4)$ [14–16] and a finite $\mathcal{P}$ appears [17]. Upon further cooling, low-temperature incommensurate (LTIC) AFM order sets in at $T_3 = 19$ K with $\mathbf{q}_{\rm LTIC} = (0.48, 0, 0.29)$ [14,18]. This transition is connected to a sign change and a reduction in magnitude of $\mathcal{P}$ [17]. The macroscopic $\mathcal{P}$ is directed along the b-axis, which requires that the symmetry has to be reduced to at least $Pb2_1m$, which allows, e.g., the structural (1, 0, 0) reflection [19].

2 Experimental

The YMn_2O_5 single crystals used for our study were grown using the PbO-PbF_2 flux method [20] and characterized by specific heat, magnetization and x-ray diffraction measurements, which were all in excellent agreement with previously published results [11,12,21]. For the RSXS experiments, a YMn_2O_5 sample with a (201)-surface normal was polished using 0.1 μm diamond films. Experiments were performed at the UE46-PGM1 beamline of BESSY II at the Helmholtz-Zentrum Berlin and the X1A2 beamline at the NSLS, Brookhaven National Laboratory. The former setup realizes a horizontal scattering experiment with variable incoming polarization and is equipped with a photodiode point detector. The scattering plane of the NSLS-chamber was vertical and the incoming polarization horizontal. In this latter case, two-dimensional cuts in reciprocal space were recorded using a Princeton Instruments PI-MTE CCD. In each case, the sample was cooled using a liquid helium flow cryostat.

3 RSXS lineshapes

To study the resonant scattering in the C-phase, we performed so-called $\theta 2\theta$-scans at different photon energies, E, across the Mn $L_{2,3}$- and O K edges at UE46. We fitted each $\theta 2\theta$-scan with a Lorantzian-squared peak shape plus a linear background. The left and right panels of Fig. 1 show the resonance at the O K- and Mn $L_{2,3}$ edges, respectively, with the main resonance features marked by vertical lines.

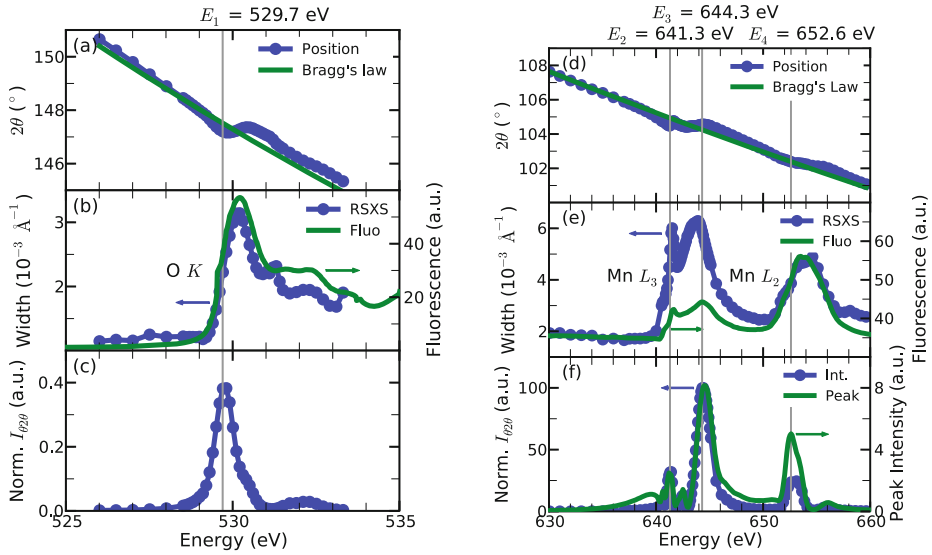

Fig. 1. Blue symbols: Energy dependent peak position (a,d), width (b,e) and integrated intensity (c,f) of $\theta 2\theta$-scans at $(1/2, 0, 1/4)$ in YMn_2O_5 at the O K- (a-c), and Mn $L_{2,3}$ edges (d-f) at 30 K. The incoming light (π) and the b-axis were in the scattering plane. The calculated position following a simple Bragg's law is shown as a solid green line in (a,d). The fluorescence was measured at 8 K, green solid line in (b,e). The peak intensity, green solid line in (f), is the peak intensity measured at the calculated Bragg position.

At resonance, the peak position deviates from Bragg's law, $2d \sin\theta = \lambda$ (cf. Fig. 1), due to the energy dependent deviation of the index of refraction, n, from 1 in the vicinity of resonant energies [22–24]. Therefore the modified Bragg's law, $2d\sqrt{n^2 - \cos^2\theta} = \lambda$, has to be used. Where $d = 2\pi/|\mathbf{q}|$, θ and $\lambda = hc/E$ are the spacing corresponding to $\mathbf{q}$, the Bragg angle and the wavelength corresponding to E, respectively. The energy dependent peak position is thus a good method to measure the often unknown n [22].

Since YMn_2O_5 has a longer correlation length of the magnetic structure than the limited penetration depth of the X-rays at these energies, the width of the reflection at a given energy is given by the probed sample volume, *i.e.*, the probing depth. Indeed the E dependent peak width gives a good measure of the X-ray absorption (XAS) cross section [Figs. 1 (b,e)]. This method provides the same bulk sensitivity as the conventional fluorescence yield measurements of the XAS, but without any self-absorption corrections. Since we are interested in the scattered intensity per volume of the resonating ions, we normalized the integrated areas at each incident energy by the probing volume, which we can estimate from the peak widths. We refer to the normalized integrated intensity as $I_{\theta 2\theta}$. At the O K edge, $I_{\theta 2\theta}$ (E) has a strong resonant enhancement at the inflection point of the XAS at $E_1 = 529.7$ eV [Figs. 1 (c)]. Furthermore we observed a shoulder on the main peak and a second smaller peak, which is similar to Ref. [25]. At the Mn $L_{2,3}$ edges, $I_{\theta 2\theta}(E)$ has strong resonant enhancements at $E_2 = 641.3$ eV, $E_3 = 644.3$ eV, and $E_4 = 652.6$ eV in the vicinity of the Mn L_3- and the Mn L_2 edges [Figs. 1 (e,f)]. This complex structure of the lineshape is governed by the multiplet structure, and is in very good agreement with other detailed RSXS studies on YMn_2O_5 [26].

For the Mn $L_{2,3}$ edges, we compare the peak intensity, I_{peak}, measured at the positions defined by Bragg's law to $I_{\theta 2\theta}$ [Fig. 1 (f)]. It can be observed that the two

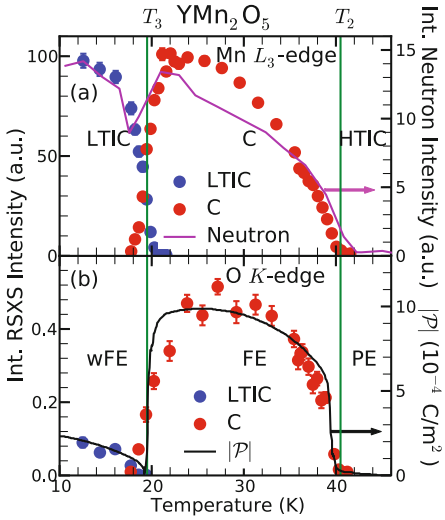

Fig. 2. Temperature dependence of the soft x-ray integrated intensity as measured at the Mn L_3- (a) and O K edges (b). The commensurate and incommensurate peaks are clearly distinguished and coexist around T_3. Good agreement is seen with the reported (solid lines) integrated intensity observed by neutron diffraction data (a) [14] and magnitude of the electric polarization $|\mathcal{P}|$ (b) [17], respectively. The phases are low temperature incommensurate (LTIC) weak ferroelectric (wFE), commensurate (C) ferroelectric (FE) and high temperature incommensurate (HTIC) paraelectric (PE).

quantities exhibit different lineshapes and, in particular, display different ratios of $I(E_3)$ (Mn L_3) and $I(E_4)$ (Mn L_2), the so-called branching ratio. The data presented in Fig. 1 therefore illustrates that for a detailed lineshape analysis $I_{\theta 2\theta}$ needs to be determined, because I_{peak} does not correctly reflect the variation of the resonant structure factor.

4 Temperature dependence

To accurately obtain the full integrated intensity in the 3D reciprocal space, $I_{3\mathrm{D}}$, we used the CCD area detector at X1A2. As a function of temperature, $I_{3\mathrm{D}}$ at E_3 (Mn L_3) tracks the neutron scattering signal [Fig. 2 (a)], demonstrating that we are measuring the magnetic order of the Mn-sublattice at this photon energy. In contrast, $I_{3\mathrm{D}}$ measured at E_1 (O K) tracks the magnitude of the FE polarization, $|\mathcal{P}|$ [Fig. 2 (b)]. In order to establish these relationships, the correct determination of $I_{3\mathrm{D}}$ is important [10]. For example, I_{peak} at the Mn L_3 edge does not recover the same intensity in the LTIC-phase as in the C-phase, in contrast to $I_{3\mathrm{D}}$. This was even more critical for the O K edge, where capturing the full integrated intensity was essential to establish the proportionality of the oxygen superstructure and $|\mathcal{P}|$.

The peak positions at the Mn $L_{2,3}$- and O K edges coincide for all temperatures and are in good agreement with the reported positions by neutron scattering [14–16,18]. Thanks to the high resolution and the high count rate of the peak, there was no problem in distinguishing the coexisting C- and LTIC-peaks around T_3 (Fig. 2).

5 Origin of the RSXS at the O K edge

It is well known that the strong X-ray magnetic circular dichroism (XMCD) at the transition metal (TM) $L_{2,3}$ edges results from the spin-orbit interaction of the $2p$

core-holes [27]. More specifically, this spin-orbit interaction implies that the $L_{2,3}$-absorption of a given TM-site depends on the projection of its local spin onto the beam direction. Since the imaginary part of the resonant scattering factor is directly related to the X-ray absorption cross section by the optical theorem [28], the XMCD further implies that the resonant scattering at the TM $L_{2,3}$ edges depends on the spin direction of the TM-sublattice. The XMCD is therefore directly related to the spin-sensitivity of RSXS at the TM $L_{2,3}$ edges. The good agreement between the magnetic neutron scattering and RSXS in Fig. 2 highlight this spin sensitivity at the TM $L_{2,3}$ edges.

At the O K edge, however, there is no spin-orbit interaction of the 1s core hole. For this reason, no strong XMCD signal due to a possible spin-moment at oxygen is expected. Nonetheless, a clear circular dichroism in the absorption at the O K edge has been observed experimentally in a number of TMO compounds [29,30]. In contrast to the TM $L_{2,3}$ edges, however, the circular dichroism in the O K edge absorption was found to be due to orbital moments, not spin-moments. These moments are transferred to oxygen by hybridization [29,30]. Based on general symmetry arguments [28], such orbital moments also cause a dichroism in absorption and therefore, again by virtue of the optical theorem, a dependence of the resonant scattering length on the direction of the (magnetic) orbital moment at oxygen. As a result, the corresponding part of the resonant scattering factor of oxygen depends directly on the hybridization between oxygen and manganese as well as on the direction of the transferred orbital moment. We note that a very similar conclusion was drawn in a previous resonant elastic X-ray scattering (REXS) study of the AFM modulation vector on UGa_3 at the Ga K edge [31].

As we have shown in our previous publication [10], the hybridization between the oxygen and the manganese is directly affected by the spin order on the manganese sublattice. The Mn-O hybridization is modulated by the magnetic order, which naturally explains in other words, why the modulation observed at the O K edge is directly related to the magnetic modulation vector, $\mathbf{q}_C$, of the Mn-sublattice. It is important to realize here that the alternating sign of the orbital moment is crucial for the appearance of the oxygen superstructure at $\mathbf{q}_C$. A simple modulation of charge density modulation by only FM-FM and FM-AFM Mn moments that is insensitive to the direction of the Mn moments would result in a peak at $2{\cdot}\mathbf{q}_C$ In fact, following the magnetic modulation, the transferred orbital moment at the oxygen site is expected to reverse sign, thus leading to a superlattice corresponding to $\mathbf{q}_C$.

The experimentally established proportionality of the RSXS at the O K edge and $|\mathcal{P}|$ shows that the spin-dependent Mn-O hybridization is directly related to the ferroelectric polarization of YMn_2O_5. The present RSXS data for the O K edge therefore constitute the direct observation of a modulation of the oxygen valence states, one that is directly connected to the magnetism and the ferroelectric polarization. Note that this method is insensitive to small structural distortions and almost exclusively probes electronic modulations. It is likely that electronic modulations as observed in the present study also play an important role for other correlated multiferroic TMOs.

6 Summary

In summary, we have shown that measuring $\theta 2\theta$-scans at different photon energies enables one to obtain the correct RSXS lineshapes, which are essential for detailed analysis of the spectroscopic information contained in these data. Further, we demonstrated that the integrated peak intensities can be efficiently and accurately measured using CCD-area detectors. In the present case, this was vital for establishing the relationship between the RSXS intensities, and the magnetic and FE order parameters.

The magnetic signal measured at the O K edge is attributed to a transferred orbital moment at the O site due to a strong Mn-O hybridization. The observed temperature dependence hence implies that the spin-dependent Mn-O hybridization plays an important role for the multiferroicity of YMn_2O_5. Finally, we note that theoretical calculations suggested that the ionic, $\mathcal{P}_{\rm ion}$, and electronic contribution to the FE polarization, $\mathcal{P}_{\rm el}$, strongly compete in the RMn_2O_5 compounds [7]. Therefore having observed $\mathcal{P}_{\rm el}$, the present results motivate a search for other correlated multiferroics, where $\mathcal{P}_{\rm el}$ not only exists but adds constructively with $\mathcal{P}_{\rm ion}$.

Many thanks to the organizers of the REXS 2011 conference in Aussois and to Gerry Lander for helpful discussions. We thank D.S. Coburn, W. Leonhardt, W. Schoenig and S. Wirick for technical support at X1A2. S.P. and J.G. thank the DFG for the support through the Emmy Noether Program (Grant GE 1647/2-1). H.W. thanks the Funding Program for World-Leading Innovative R&D on Science and Technology (FIRST Program). Work performed at BNL was supported by the US Department of Energy, Division of Materials Science, under contract No. DE-AC02-98CH10886.

References

1. S.-W. Cheong, M. Mostovoy, Nat. Mater. **6**, 13 (2007)
2. D. Khomskii, Physics **2**, 20 (2009)
3. T. Kimura, T. Goto, H. Shintani, K. Ishizaka, T. Arima, Y. Tokura, Nature **426**, 55 (2003)
4. N. Hur, S. Park, P.A. Sharma, J.S. Ahn, S. Guha, S-W. Cheong, Nature **429**, 392 (2004)
5. C. Wang, G.-C. Guo, L. He, Phys. Rev. Lett. **99**, 177202 (2007)
6. A.S. Moskvin, S.-L. Drechsler, Phys. Rev. B **78**, 024102 (2008)
7. G. Giovannetti, J. van den Brink, Phys. Rev. Lett. **100**, 227603 (2008)
8. A.S. Moskvin, R.V. Pisarev, Phys. Rev. B **77**, 060102 (2008)
9. T. Lottermoser, D. Meier, R.V. Pisarev, M. Fiebig, Phys. Rev. B **80**, 100101 (2009)
10. S. Partzsch, S.B. Wilkins, J.P. Hill, E. Schierle, E. Weschke, D. Souptel, B. Büchner, J. Geck, Phys. Rev. Lett. **107**, 057201 (2011)
11. M. Tachibana, K. Akiyama, H. Kawaji, T. Atake, Phys. Rev. B **72**, 224425 (2005)
12. S. Quezel-Ambrunaz, F. Bertaut, G. Buison, C. R. Acad. Sc. Paris **258**, 3025 (1964)
13. S.C. Abrahams, J.L. Bernstein, J. Chem. Phys. **46**, 3776 (1967)
14. I. Kagomiya, H. Kimura, Y. Noda, K. Kohn, J. Phys. Soc. Jpn. **70(A)**, 145 (2001)
15. Y. Noda, H. Kimura, Y. Kamada, T. Osawa, Y. Fukuda, Y. Ishikawa, S. Kobayashi, Y. Wakabayashi, H. Sawa, N. Ikeda, K. Kohn, Physica B **385-386**, 119 (2006)
16. C. Vecchini, L.C. Chapon, P.J. Brown, T. Chatterji, S. Park, S.W. Cheong, P.G. Radaelli, Phys. Rev. B **77**, 134434 (2008)
17. Y. Noda, Y. Fukuda, H. Kimura, I. Kagomiya, S. Matumoto, K. Kohn, T. Shobu, N. Ikeda, J. Korean Phys. Soc. **42**, 1192 (2003)
18. P.G. Radaelli, C. Vecchini, L.C. Chapon, P.J. Brown, S. Park, S.-W. Cheong, Phys. Rev. B **79**, 020404 (2009)
19. I. Kagomiya, S. Matsumoto, K. Kohn, Y. Fukuda, T. Shoubu, H. Kimura, Y. Noda, N. Ikeda, Ferroelectrics **286**, 167 (2003)
20. B.M. Wanklyn, J. Mater. Sci. **7**, 813 (1972)
21. A. Ikeda, K. Kohn, Ferroelectrics **169**, 75 (1995)
22. L. Seve, J.M. Tonnerre, D. Raoux, J. App. Cryst. **31**, 700 (1998)
23. M. Sacchi, C.F. Hague, L. Pasquali, A. Mirone, J.-M. Mariot, P. Isberg, E.M. Gullikson, J.H. Underwood, Phys. Rev. Lett. **81**, 1521 (1998)
24. H.-C. Mertins, O. Zaharko, A. Gaupp, F. Schäfers, D. Abramsohn, H. Grimmer, J. Magn. Magn. Mater. **240**, 451 (2002)

25. T.A.W. Beale, S.B. Wilkins, R.D. Johnson, S.R. Bland, Y. Joly, T.R. Forrest, D.F. McMorrow, F. Yakhou, D. Prabhakaran, A.T. Boothroyd, P.D. Hatton, Phys. Rev. Lett. **105**, 087203 (2010)
26. R.A. de Souza, U. Staub, V. Scagnoli, M. Garganourakis, Y. Bodenthin, S.-W. Huang, M. García-Fernández, S. Ji, S.-H. Lee, S. Park, S.-W. Cheong, Phys. Rev. B **84**, 104416 (2011)
27. G. van der Laan, Phys. Scr. **41**, 574 (1990)
28. S.P. Collins A. Bombardi, *Magnetism and Synchrotron Radiation*, Chap. 8 (Springer, 2010)
29. E. Pellegrin, L.H. Tjeng, F.M.F. de Groot, R. Hesper, G.A. Sawatzky, Y. Moritomo, Y. Tokura, J. Phys. IV (France) **7(C2)**, 405 (1997)
30. E. Goering, A. Bayer, S. Gold, G. Schütz, M. Rabe, U. Rüdiger, G. Güntherodt, Europhys. Lett. **58**, 906 (2002)
31. D. Mannix, A. Stunault, N. Bernhoeft, L. Paolasini, G.H. Lander, C. Vettier, F. de Bergevin, D. Kaczorowski, A. Czopnik, Phys. Rev. Lett. **86**, 4128 (2001)